Catena 199 (2021) 105108

Contents lists available at ScienceDirect

Catena

journal homepage: www.elsevier.com/locate/catena

Performance of bedload transport equations in a mixed bedrock–alluvial channel environment

Guilherme Kruger Bartels [a,*], Nilza Maria dos Reis Castro [a], Gilberto Loguercio Collares [b], Fernando Mainardi Fan [a]

[a] Instituto de Pesquisas Hidráulicas, Universidade Federal do Rio Grande do Sul (Institute of Hydraulic Research, Federal University of Rio Grande do Sul – IPH/UFRGS), Av. Bento Gonçalves, 9500 Porto Alegre, RS, Brazil
[b] Centro de Desenvolvimento Tecnológicos, Universidade Federal de Pelotas (Center for Technological Development, Federal University of Pelotas – CDTec/UFPel), Rua Gomes Carneiro 01, Pelotas, RS, Brazil

ARTICLE INFO

Keywords:
Bedload transport
Bedrock
Macro-roughness
Bedload rating curve
Flow resistance
Limited sediment mobility

ABSTRACT

Mixed bedrock–alluvial channel beds are common in mountain rivers. It is well-known that in such system the balance between sediment supply and transport capacity defines either the level of the exposure of bedrock (in the riverbed) or its coverage by alluvial material. We investigate whether applying the representation of the energy losses (caused by macro-roughness) developed for alluvial channels improve the capacity of bedload transport equations to predict the bedload transport in a mixed bedrock–alluvial stream. Therefore, the purpose of this study was to evaluate the performances of five bedload equations against field measurements, while considering the effects of macro-roughness on the equations and the limited availability of mobile sediment. We analyzed the data collected in a stream located in southern Brazil, which has a 2.3% gradient and mixed bed conditions. Optimal results in estimating the bedload transport rate were obtained when using the reduced shear stress ($\tau^{'}$) and reduction factor of the available bed material (*Frm*) together in the five tested equations. Analyzing the two approaches separately, the implementation of $\tau^{'}$ proved to be more critical for improving the performance of the equations than using *Frm* alone. Among all the equations, Recking (2013) presented the best result for the case in which 85.2% of the estimates fell within one order of magnitude of the measured transport rates ($0.1 < r > 10.0$); this was followed by the Recking (2010) (70.4% of estimates within one order of magnitude) and Meyer-Peter and Müller (1948) (37% of estimates within one order of magnitude) equations. In conclusion, we observed that even by implementing flow resistance and with the limited availability of mobile sediment, the equations overestimated the bedload transport rate in the studied river reach, indicating an underestimation of energy loss in the flow resistance equations of mixed bedrock–alluvial channels.

1. Introduction

Mixed bedrock–alluvial channel beds are common in mountain rivers and are characterized not only by patches of exposed bedrock but also by the degree of alluvial cover (Turowski et al., 2008). The balance between sediment supply and transport capacity determines the exposure of bedrock in a riverbed or its alluvial material cover, and if the bedload transport capacity of the river exceeds its bed sediment supply, the bedrock will eventually be exposed (Ferguson et al., 2017b).

The sediments in bedrock rivers are generally transported across alluvial and bedrock surfaces (Hodge et al., 2011), presenting a pattern and depth of sediment cover that vary over time (Zhang et al., 2015).

Abbreviations: GSD, grain-size distribution; DGPS, differential global positioning system; Q_b, Bedload transport rate; d/D, relative flow depth; Cfa, humid subtropical climate; B, Boulder; bC, boulder-Cobble; bcG, boulder-cobble-Gravel; cG, cobble-Gravel; G, Gravel; gbC, gravel-boulder-Cobble; gS, gravel-Sand; sG, sand-Gravel; Q, water discharge; A, flow area; W, flow width; P, wetted perimeter; R, hydraulic radius; d, mean flow depth; v, mean flow velocity; h, stage; VPE, variable power equation; Ferg2007, VPE from Ferguson (2007); RR2011, Rickenmann and Recking (2011); WC-2003, Wilcock and Crowe (2003); MPM-1948, Meyer-Peter and Müller (1948); Rn-2001, Rickenmann (2001); Rg-2010, Recking (2010); Rg-2013, Recking (2013); $q_{b\ meas}$, measured unit bedload transport rate; $q_{b\ cal}$, estimated unit bedload transport rate; *r*, discrepancy ratio; *mr*, arithmetic mean of *r*.

* Corresponding author.
E-mail addresses: guilhermebartels@gmail.com (G.K. Bartels), nilza@iph.ufrgs.br (N.M.R. Castro), gilbertocollares@gmail.com (G.L. Collares), fernando.fan@ufrgs.br (F.M. Fan).

https://doi.org/10.1016/j.catena.2020.105108
Received 30 April 2020; Received in revised form 8 December 2020; Accepted 14 December 2020
Available online 29 December 2020

Several studies that have focused on bedrock incision have used models to predict bed fractions with alluvial cover (Chatanantavet and Parker, 2008; Hodge and Hoey, 2012; Inoue et al., 2014; Johnson, 2014; Sklar and Dietrich, 2004; Turowski et al., 2007; Zhang et al., 2015). In these models, the sediment cover is parameterized in terms of average sediment supply and transport capacity (Chatanantavet and Parker, 2008; Sklar and Dietrich, 2004; Turowski et al., 2007) and is controlled by the bedrock surface roughness (Inoue et al., 2014; Johnson, 2014; Zhang et al., 2015). As the topographic roughness of the bedrock is intrinsic to natural channels, its variability affects the extent and pattern of alluvial cover (Inoue et al., 2014).

Thus, the rate of sediment transport and the sediment grain sizes in mixed bedrock–alluvial channels are influenced by the surface roughness, the proportion and distribution of alluvial and bedrock surfaces, and the flow velocity profile of the channels (Hodge et al., 2011). Many bedload transport equations, originally developed with data from flume experiments and under uniform bed material, generally overestimate the rate of sediment transport in streams with coarse bed material and a high slope by several orders of magnitude (Nitsche et al., 2011; Rickenmann, 2001). Thus, it is reasonable to say that the equations applied to mixed bedrock–alluvial channels should consider the proportion of alluvial cover and must also consider the estimated bed roughness height.

Mountain regions feature river channels with longitudinal gradients >0.2% (Wohl, 2010). These streams have characteristics including wide grain-size distribution (GSD) of bed material (i.e., from sand to rarely mobile boulders) (Monsalve et al., 2016; Yager et al., 2012a), reduced relative flow depth (d/D, where d is the mean flow depth and D is the characteristic grain size) (Comiti and Mao, 2012), large boulders that remain immobile even during high flows (Nitsche et al., 2011), and varying channel widths (Nitsche et al., 2011; Schneider et al., 2015a). All these features produce resistance due to additional roughness, which is absent in channels with reduced slopes and which is hardly considered in laboratory conditions (Nitsche et al., 2011).

Considering the effects of flow resistance caused by the prominent elements mentioned previously (i.e., macro-roughness), energy losses are often described using empirical equations based on the measurements of these elements, such as the characteristic grain size D_{84} (84th percentile of the GSD) (Rickenmann and Recking, 2011), D_{65} (65th percentile of the GSD) (Wilcock et al., 2009), or the dimensions/concentrations of boulders and protrusions (Yager et al., 2012a, 2007). Moreover, in steep streams, the availability of sediments is often limited due to the presence of coarse grains that have immobile characteristics in stream beds (Yager et al., 2012a, 2012b). In other words, besides the availability of finer sediments for transport, the fraction of coarse grains relative to the amount of permanently immobile sediments and bedrock determines the availability of coarse grains for transport (Yuill et al., 2010). Studies using tracers show much greater sediment mobility (and with no selectivity in size) in bedrock sections and a trend of being less mobile and more selective from the sediment cover (partial) to the alluvial cover (Ferguson et al., 2017b; Hodge et al., 2011).

Recent studies have shown that the performance of bedload equations for alluvial channels has improved because they now include the effects of energy losses due to the resistance caused by bed macro-roughness (Green et al., 2015; Schneider et al., 2016, 2015; Yager et al., 2007) and the limited availability of mobile bed material (Green et al., 2015; Yager et al., 2007). Although coarse bed alluvial channels have characteristics in common with bedrock rivers (Whipple et al., 2013), we investigate whether the representation of the energy loss caused by macro-roughness and the limited sediment mobility developed for alluvial channels can be applied to increase the performance of bedload transport equations under conditions that contrast with those applied initially. Thus, we were motivated to perform field measurements of bedload transport under varying flow conditions. This study evaluated the performance of five bedload equations previously developed for alluvial streams, considering the macro-roughness effects and limited sediment mobility present in a mixed bedrock–alluvial stream.

2. Material and methods

2.1. Study site

We selected the Arroio do Ouro watershed, which is located in the state of Rio Grande do Sul in Brazil, as the study area (Fig. 1a). The watershed has a drainage area of 17.17 km^2; the elevation varies from 76 to 326 m above sea level, and the area has a mean slope of 13% (0.13 m m^{-1}) and up to 58% (0.58 m m^{-1}). The region covers the Pelotas Batholith (i.e., a plutonic complex that includes granite, gabbro, and diorite), the geological unit of the Dom Feliciano Belt, and the eastern portion of the Sul-rio-grandense Shield (Philipp et al., 2016b, Philipp et al., 2016a). The soils of the Arroio do Ouro watershed are classified (FAO Taxonomy) as Acrisols and Regosols (FAO, 2014), which are shallow and predominantly contain sandy loam (35–75% sand) (Bartels et al., 2016).

According to the Köppen system, the climate in the region is Cfa, which is characterized by a humid subtropical climate with hot summers and well-distributed rain throughout the year (Peel et al., 2007). During the period between 1971 and 2018, annual rainfall was 1400 ± 299 mm, annual reference evapotranspiration was 1077 ± 33 mm, and the mean annual temperature was 18.5 ± 0.5 °C. We selected the catchment and river reach areas as they are considered areas that are representative of existing natural streams in the region.

2.2. Mapped reach and grain size

We mapped a reach area (in the Arroio do Ouro stream) that was 66 m long and approximately 5.5 m wide, directly upstream from the cross-section where water discharge and bedload transport rate measurements were taken. Water discharge (Q) and total bedload transport (Q_b) were recorded. The reach has a bed gradient of 0.023 m m^{-1} (Fig. 1e). We used a total station and a differential global positioning system (DGPS) to measure the bed topography (average of 7 points/m^2; Fig. 1c) and mapped the boundaries of all the patches (Fig. 1d) which were visually identified by observing sharp changes in the GSD of the bed material. The mapped reach of the river consisted of sediments with wide GSDs (from large boulders [Fig. 2c] to sand and gravel [Fig. 2a, 2b]) in addition to bedrock (Fig. 2a, b).

Patches were grouped into eight different classes using the classification scheme of Buffington and Montgomery (1999) and were considered in addition to the bedrock (Fig. 1d). The textural patches are listed in the order of increasing surface sediment grain sizes, namely, sand (<2 mm), gravel (2–63 mm), cobble (64–256 mm), and boulders (>256 mm) (Yager et al., 2012). A second or third class was inserted only if the predominant class presented < 90% of the total, e.g., the boulder–-gravel–Cobble (bgC) group is mainly composed of cobble, followed by gravel (>5%) and boulders (>5%) (Buffington and Montgomery, 1999).

The bed grain size was mostly determined using a sampling frame method, in which elastics presented in the grid way interior indicate the particles that are included in the sample (Bunte and Abt, 2001). However, in some cases, pebble counts were performed with grains that were selected during random walks (Wolman, 1954). For these methods, the b-axis of each particle was directly measured using a gravel template (gravelometer) with a progressive square aperture of 0.5 phi (Bunte et al., 2009; Bunte and Abt, 2001), which eliminates possible operating errors that can occur while measuring grain sizes (Bunte et al., 2009). A tape was used to measure the sizes of larger grains and bedrock protrusions. A total of 2135 grains were measured, with at least one standard pebble count (100 grains) conducted for each patch class. As the protruding bedrock in the stream bed is an immobile flow obstacle, we considered it in the GSD of the bed material and used it as a parameter of the measured vertical distance (i.e., from the top of the protrusion to the average adjacent bed surface) (Fig. 2d). Thus, we included protrusions

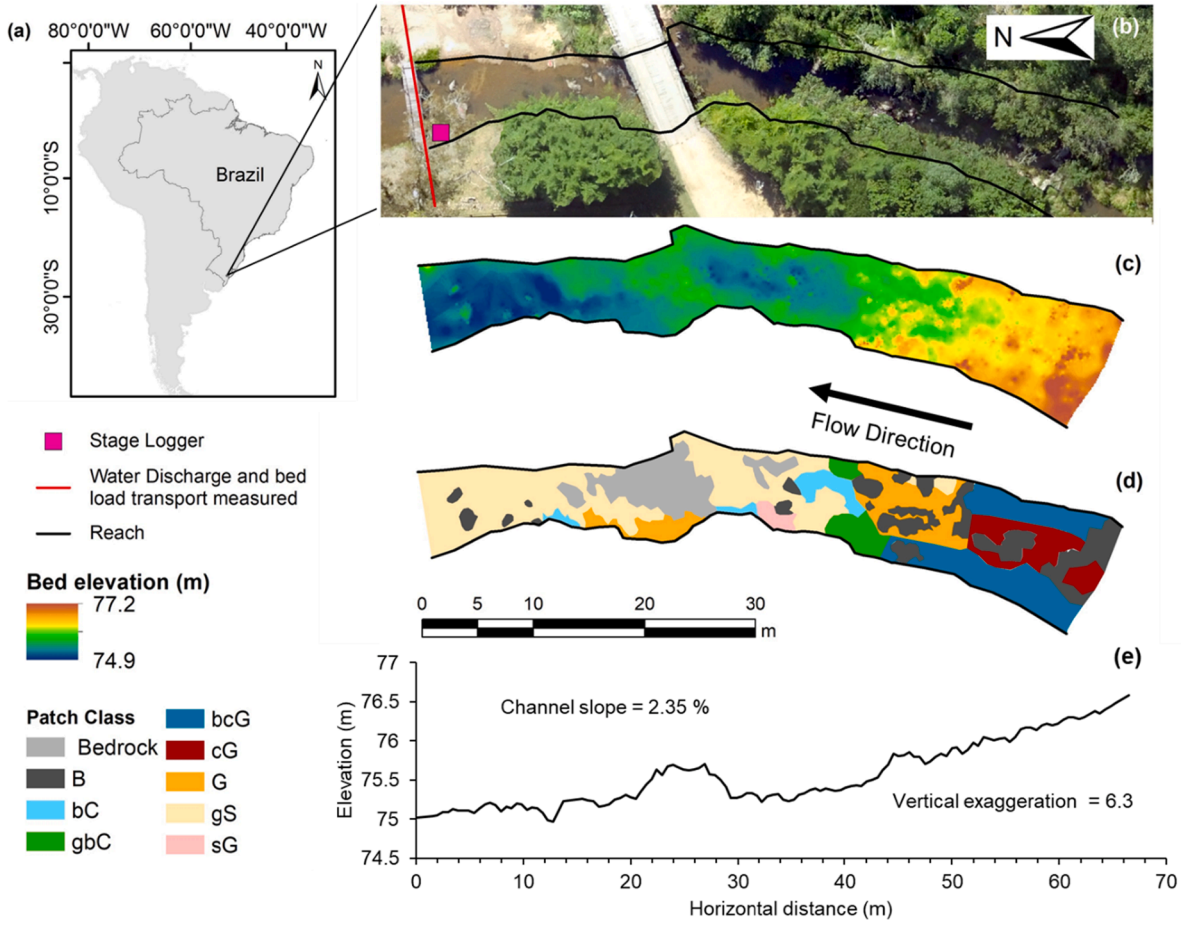

Fig. 1. (a) Location of the study area, Rio Grande do Sul, Brazil; (b) Arroio do Ouro stream reach showing the channel cross-section where water discharge and bedload transport measurements were taken; (c) bed elevation surveyed from total station and a differential global positioning system (DGPS); (d) map of patches: Boulder (B), boulder–Cobble (bC), gravel–boulder–Cobble (gbC), boulder–cobble–Gravel (bcG), cobble–Gravel (cG), Gravel (G), gravel–Sand (gS), sand–Gravel (sG), and; (e) longitudinal profile of thalweg.

into boulder patches (considered here as immobile). In the patch classes that contained sand (i.e., gS and sG), the surface bed material was collected and transported to the laboratory where the GSDs were estimated by sieving the material using a progressive mesh of 0.5 phi.

We determined the GSD for each patch class as the sum of the area-weighted pebble counts within that patch class (Table 1). Classes with predominantly the same grain size (i.e., sG, G, cG, and bcG) also had similar median diameters (D_{50}). However, there were substantial differences in D_{84}, thereby characterizing the importance of mapping coarse sediments, even though they had a lower frequency than that observed in the dominant class (Table 1).

The D_{84}/D_{50} ratio is indicative of a sorted sediment bed (Millar, 1999). Eight patch classes had ratios between 1.7 and 3.9, and similar values were found for the same classes in other studies (Monsalve et al., 2016; Yager et al., 2012a). Considering the entire bed (i.e., "Total" values in Table 1), the D_{84}/D_{50} ratio was approximately 20, which is much higher than the ratios found in other studies that considered coarse beds (Monsalve et al., 2016; Rickenmann, 2018; Schneider et al., 2016; Yager et al., 2012a, 2012b). This is due to the wide range of grain sizes present in the bed, i.e., from large boulders to sand and gravel (Fig. 2). In addition, the classes with sand (i.e., gS and sG) had a proportional area of 34%, and classes with boulders (i.e., B, bC, bcG, and gbC) were distributed throughout 38% of the entire bed (Table 1). The similar area-weighted values calculated in different grain sizes resulted in a less steep curve of the bed material GSD compared to the GSD of the transported particles (Fig. 3).

2.3. Flow property measurements

We measured 55 discharges from March 2013 to July 2015 using a traditional current meter (Turnipseed and Sauer, 2010). We used the flow velocity measured into series of 0.5 m or 1.0 m vertical spacings to quantify the water discharge (Q), flow area (A), flow width (W), and wetted perimeter (P) in the cross section. From these data we calculated the hydraulic radius ($R = A/P$), mean flow depth ($d = A/w$), and mean flow velocity ($v = Q/A$). Continuous stage records were obtained using a pressure transducer (Fig. 1).

We constructed stage-discharge rating curves with the stage (h) varying from 0.29 to 1.45 m, resulting in a discharge interval that varied from 0.12–14.84 $m^3\ s^{-1}$ (Fig. 4a). For a better data fit, the rating curve was divided into two segments, representing discharges with $h < 0.78$ m and flows with $h > 0.78$ m; both situations presented an excellent fit ($r^2 = 0.99$).

The tendencies of the flow velocity and flow depth to increase with the discharge (in cross section) is well defined in Fig. 4b and c. The rate of change in flow velocity with discharge was greater than the rate of change in flow depth. This reflects the flow resistance decrease with increased discharge because sources of grain and form roughness occupy a progressively smaller portion of the flow (David et al., 2010a). The power function fitted by ordinary least squares had exponents of 0.55 for flow velocity and 0.18 for flow depth. These results are consistent with other studies of bedrock channels (Ferguson et al., 2017a) and steep alluvial streams (Comiti et al., 2007; David et al., 2010a).

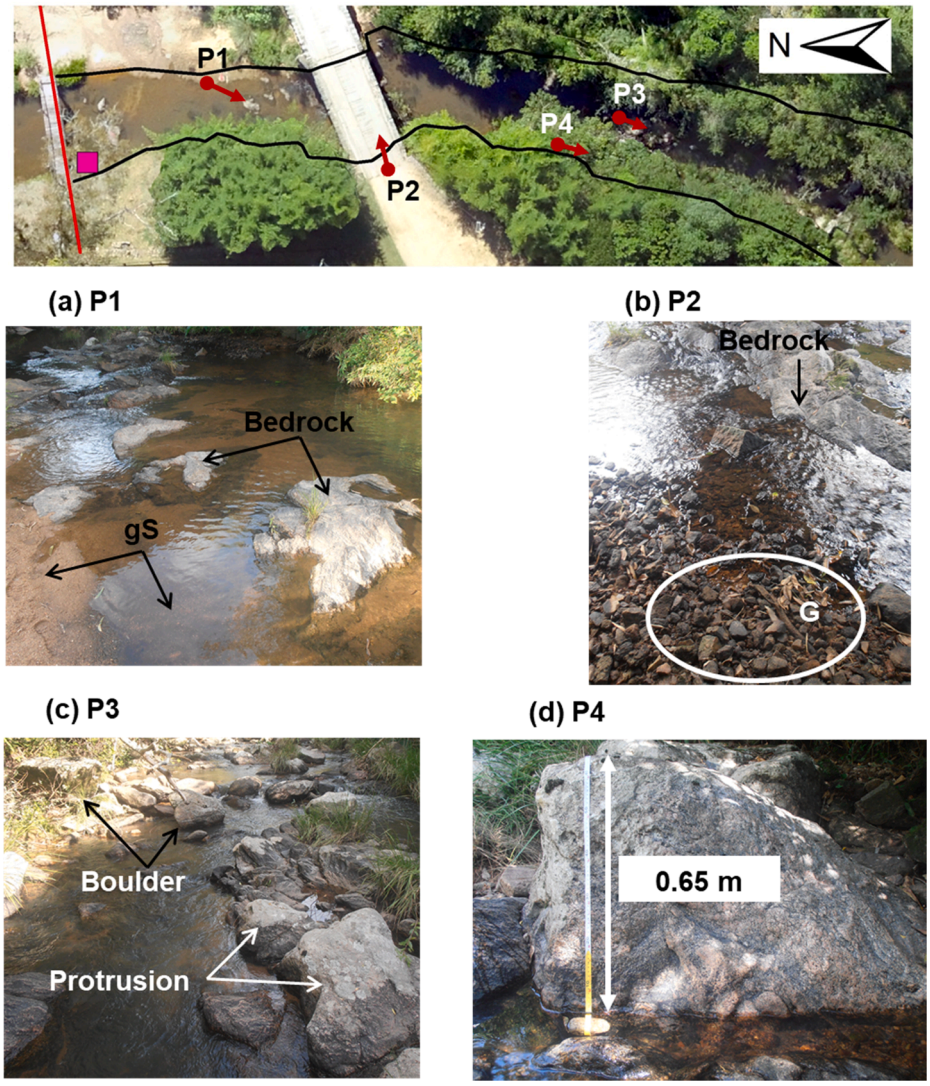

Fig. 2. Locations of photographs (P1, P2, P3, and P4): (a) P1 bed with fine sediments (gravel–Sand [gS]) and bedrock; (b) P2 showing a gravel-bed (Gravel [G]) and bedrock; (c) P3 showing a coarser bed (Boulder [B]) and bedrock protrusion; (d) P4, an example of a bedrock protrusion measurement.

Table 1
Characteristics of textural patches in the mapped reach of Arroio do Ouro stream.

	Class	D_{50} (mm)	D_{84} (mm)	D_{84}/D_{50}	A_p
B	Boulder	525	891	1.7	0.14
bC	boulder–Cobble	215	374	1.7	0.04
bcG	boulder–cobble–Gravel	33	128	3.9	0.16
cG	cobble–Gravel	21	69	3.3	0.07
G	Gravel	19	40	2.1	0.10
gbC	gravel–boulder–Cobble	116	268	2.3	0.04
gS	gravel–Sand	0.9	1.9	2.1	0.33
sG	sand–Gravel	11	32	2.9	0.01
	Bedrock	–	–	–	0.12
	Mobile	**7**	**81**	**10.9**	**0.74**
	Total	**16**	**333**	**20.4**	**1.00**

D_{50} and D_{84} indicate the 50th and 84th percentiles in grain diameter, respectively (for each patch class).
A_p represents the proportional area of each class in the studied reach.
"Total" represents the entire bed.

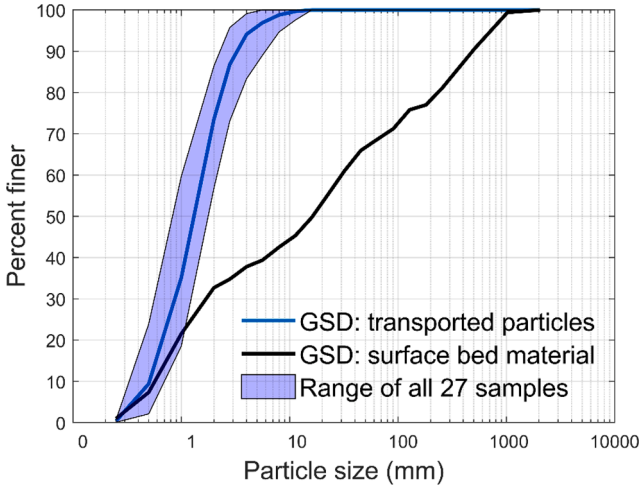

Fig. 3. Grain-size distribution (GSD) of the surface bed material and transported particles. The average bedload GSD (blue line) was based on all 27 collected samples (represented by the shaded region). (For interpretation of the references to color in this figure legend, the reader is referred to the web version of this article.)

2.4. Bedload transport measurement

A total of 27 samples of bedload transport were collected from June 2014 to July 2015, with discharge measurements obtained under

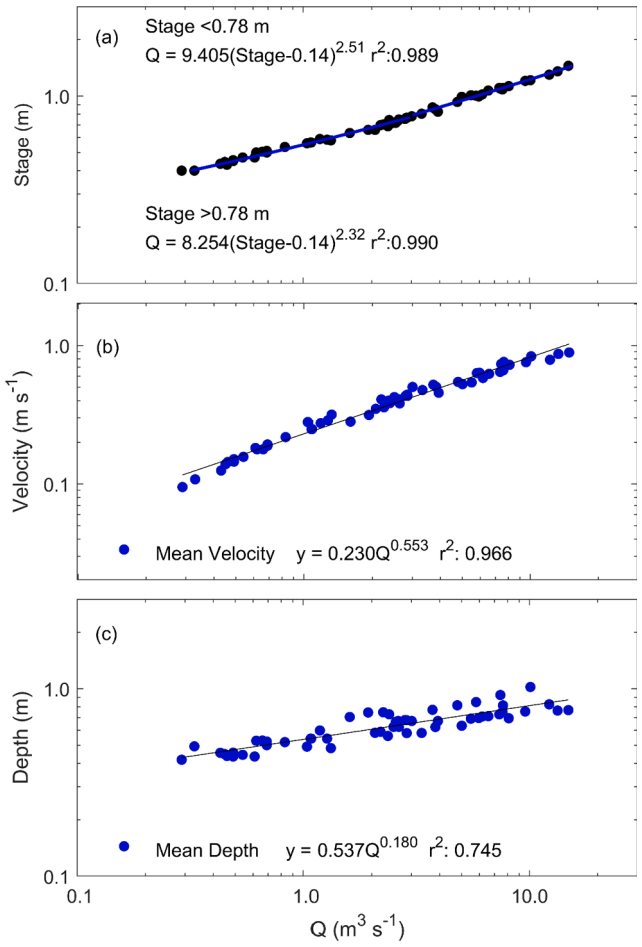

Fig. 4. (a) Hydraulic relationships between discharge and stage; (b) mean flow velocity; and (c) mean flow depth of Arroio do Ouro stream cross-section.

varying flow conditions (see Fig. 5). We used a Helley–Smith sampler (Helley and Smith, 1971) with a 76 × 76-mm nozzle and a bag with 0.25-mm mesh openings. Each sample was measured in 4–8 equidistant verticals of the cross section, and more verticals were implemented with increased flow width. The sampler remained on the streambed for 60 s at each vertical. The bedload transport rate (Q_b) was calculated according to Eq. (1):

$$Q_b = \frac{W \times M}{W_{HS} \times n \times t}, \quad (1)$$

where Q_b is the measured bedload transport rate (kg s^{-1}), W is the width of the section (m), W_{HS} is the width of the Helley–Smith sampler (0.076 m), n is the number of verticals, M is the total dry mass of sediment collected (kg), and t is the collection time of each sample.

For pebbles < 16 mm, we used the sampling efficiency of one unit for the Helley–Smith sampler as indicated by Emmett (1980). The maximum sampled diameter was 12.5 mm (only for discharge > 2.3 m^3 s^{-1}). As this diameter is five times smaller than that of the sampler nozzle, it satisfied the minimum condition indicated by Vericat et al. (2006) for the use of the Helley–Smith sampler. Thus, the GSD of the transported particles was not considered to be a limiting factor for the quality of collected samples.

An electromagnetic stirrer equipped with sieves with a progressive mesh of 0.5 phi was used to determine the GSD of the transported particles. The bedload granulometry was finer than the GSD of the bed material (Fig. 3). Bedload samples collected during the monitored events presented a mean D_{50} of 1.4 mm (0.8 mm < D_{50} < 1.9 mm) and a mean D_{84} of 2.7 mm (1.9 mm < D_{84} < 4.2 mm).

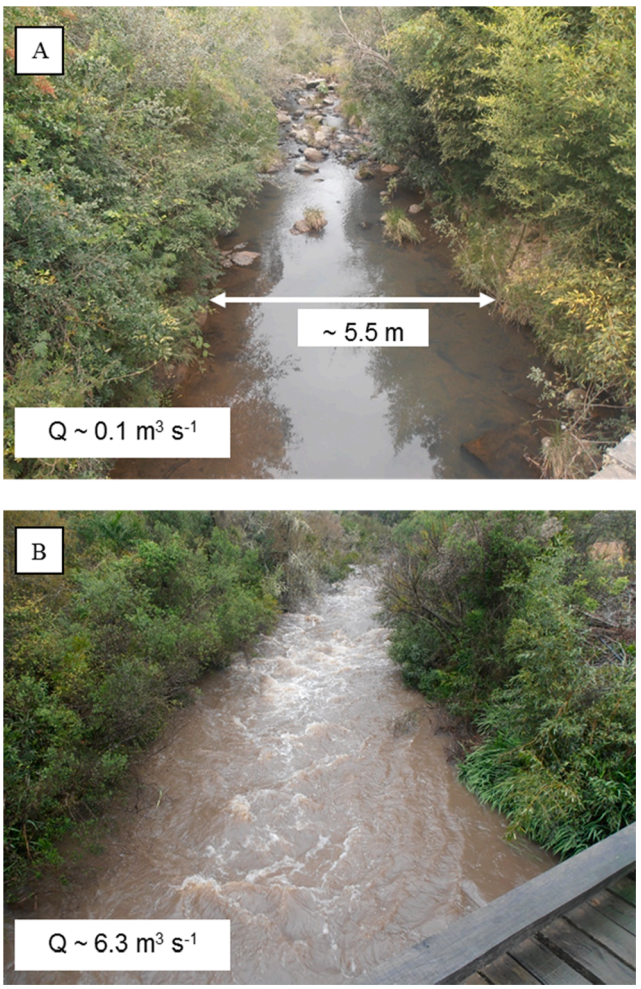

Fig. 5. Upstream view of Arroio do Ouro reach observed in: (a) low flow (approximately 0.1 m^3 s^{-1}) and (b) high flow (approximately 6.3 m^3 s^{-1}). Note the exposed bedrock protrusion and immobile boulders.

2.5. Flow resistance equations

Flow resistance relationships may be used to predict the mean flow velocity when direct measurements are not possible or available (Schneider et al., 2015b). The total flow resistance is traditionally described using the Manning, Chezy, and Darcy–Weisbach equations:

$$v = \frac{d^{2/3}\sqrt{S}}{n} = C\sqrt{dS} = \sqrt{\frac{8gdS}{f_{tot}}}, \quad (2)$$

where v is the flow velocity, n is the Manning coefficient, C is the Chezy coefficient, f_{tot} is the Darcy–Weisbach friction factor, d is the flow depth (or hydraulic radius [R] for narrow channels), S is the energy slope (or the channel bed slope), and g is the gravitational acceleration (m s^{-2}). Most equations were derived for f_{tot} because they are dimensionless coefficients (Ferguson, 2007; Rickenmann and Recking, 2011).

Using a dataset of 2890 field measurements, Rickenmann and Recking (2011) evaluated the variable power equation (VPE) developed by Ferguson (2007) and found that it has the best performance among several other flow resistance equations. Ferguson (2007) developed a single resistance equation that combined the roughness-layer formulations for shallow flows and the Manning–Strickler for deep flows. Thus, the VPE considers the friction factor (f_{tot}) as the sum of two components (i.e., grain friction and bedform effects) which are both present in coarse streambeds:

$$\sqrt{\frac{8}{f_{tot}}} = \frac{v}{u^*} = \frac{a_1 a_2 \left(\frac{d}{D_{84}}\right)}{\sqrt{{a_1}^2 + {a_2}^2 \left(\frac{d}{D_{84}}\right)^{5/3}}}, \quad (3)$$

where u^* is the shear velocity ($u^* = [gdS]^{0.5}$) and d/D_{84} is the relative flow depth. We used the empirical constant values $a_1 = 6.5$ and $a_2 = 2.5$, as suggested by Ferguson (2007) and Rickenmann and Recking (2011).

Flow resistance equations are more reliable for streams with low roughness ($d/D_{84} > 4$) as proposed by Bathurst et al. (1981) because flow turbulence is strongly affected by large bed elements (cobbles, boulders, and bedrock protrusion) observed in channels with more roughness (Rickenmann and Recking, 2011). Alternatively, regarding approaches using relative flow depth and f_{tot}, dimensionless hydraulic geometry relationships have been proposed to represent the flow velocity in steep streams (Comiti et al., 2007; Ferguson, 2007; Rickenmann and Recking, 2011). Thus, the flow velocity can be nondimensionalized as follows:

$$v^{**} = k q^{**m}, \quad (4)$$

where

v^{**} is the dimensionless velocity $v^{**} = v/(gSD_{84})^{0.5}$;
q^{**} is the dimensionless discharge $q^{**} = q/(gSD_{84}^3)^{0.5}$;
q is the unit discharge $q = Q/W$, and;
k and m are empirical constants.

Several studies have consistently demonstrated that predictions based on unit discharge provide better estimates of flow velocities in rough streams than the traditional approaches that adopt relative flow depth and f_{tot} (Comiti et al., 2007; Rickenmann and Recking, 2011; Schneider et al., 2015b; Zimmermann, 2010). Rickenmann and Recking (2011) transformed the original VPE based on relative flow depth (Eq. (3)) to an equivalent q-based form as shown in Eq. (5).

$$v^{**} = \frac{v}{(gSD_{84})^{0.5}} = 1.443 q^{**0.6} \left[1 + \left(\frac{q^{**}}{43.78}\right)^{0.8214}\right]^{-0.2435} \quad (5)$$

Based on the performance of the equation for the predicted flow velocity (see Section 3.1) and the consistent results reported in the literature (Nitsche et al., 2011; Rickenmann and Recking, 2011; Schneider et al., 2015b), we used dimensionless hydraulic geometry relationships (Eq. (5)) of Rickenmann and Recking (2011) in the flow resistance partitioning approach (see Section 2.6).

2.6. Flow resistance partitioning

Owing to the presence of macro-roughness elements (i.e., boulders and bedrock protrusion), we combined the flow resistance equation with bedload transport equations by using a reduced energy slope which is based on flow resistance partitioning instead of the actual channel slope. The total flow resistance (f_{tot}) can be considered as the sum of base-level resistance (f_o) and additional resistance ($f_{add} = 1 - f_{tot}$) caused by large roughness elements (Nitsche et al., 2011). Previous studies of bedload transport rates have used the reduced energy slope (S_{red}) in steep streams (Heimann et al., 2015; Nitsche et al., 2011; Rickenmann, 2012; Schneider et al., 2016, 2015a) as the relationship between the stream gradient, and the Darcy–Weisbach friction factor in the following way:

$$S_{red} = S\left(\sqrt{\frac{f_o}{f_{tot}}}\right)^e, \quad (6)$$

where S is the bed slope (m m^{-1}). The exponent e varies from 1 to 2, and we used a fixed value of $e = 1.5$, as established in a previous study (Nitsche et al., 2011). Based on predicting flow velocity using dimensionless variables, which provides the optimal results, we calculated the partitioning between f_o and f_{tot} as proposed by Rickenmann and Recking (2011) using the following equation:

$$\sqrt{\frac{f_o}{f_{tot}}} = \left(\frac{v(q)}{v_o(q)}\right)^{1.5}, \quad (7)$$

where v is the flow velocity obtained by Eq. (5) and v_o is the equivalent velocity that corresponds to the base-level resistance ($v_o = 3.074 q^{**0.4} [gSD_{84}]^{0.5}$) (Rickenmann, 2012; Rickenmann and Recking, 2011).

We used a reduced energy slope (Eq. (6)) to calculate the reduced shear stress (τ', [Eq. (8)]) or the dimensionless reduced shear stress ($\tau^{*'}$ [Eq. (9)]), which are functions that are typically described in bedload transport equations.

$$\tau' = \rho g R S_{red}, \quad (8)$$

$$\tau^{*'} = \frac{\tau'}{(\rho_s - \rho) g D_x}, \quad (9)$$

where ρ is the water density (kg m^{-3}), ρ_s is the sediment density (kg m^{-3}), and D_x is the grain size for which x percent of the material is fine (m).

2.7. Limited availability of mobile sediment

The reach of the Arroio do Ouro stream was partially covered with sediment classified as immobile and bedrock (Fig. 1; Table 1). Considering that these large elements of roughness were not available for transportation, we applied a reduction factor to the available bed material (*Frm*) in the bedload transport equations. This reduction factor has also been implemented in other bedload transport models (Yager et al., 2007) and is expressed as follows:

$$Frm = \frac{A_m}{A_{tot}}, \quad (10)$$

where A_{tot} is the total bed area and A_m is the bed area with mobile sediment.

2.8. Bedload transport equations

We evaluated the effects of macro-roughness and the limited availability of mobile sediment on the performance of the five equations, which were developed and previously applied in streams with sand or gravel beds (Heimann et al., 2015; López et al., 2014; Recking et al., 2016, 2012; Schneider et al., 2016, 2015a; Vázquez-Tarrío and Menéndez-Duarte, 2015). To assess the effect of macro-roughness and the limited availability of mobile sediment separately, as well as together, all equations were analyzed in four ways (Fig. 6): I- original equations, II- modified equations (τ and *Frm*), III- modified equations (only τ'), and IV- modified equations (τ' and *Frm*). The equations described below consider the effects of macro-roughness and the limited availability of mobile sediment (i.e., IV- modified equations). The original and II- and III- modified equations are available in the supplementary material.

The equation of Wilcock and Crowe (2003) (WC-2003) is based on the fractional dimensionless transport rate $W_i^{*'}$ (Eq. (11)) as a function of reduced shear stress (τ') and reference shear stress (τ_{ri}) (Eq. (12)).

$$W_i^{*'} = \frac{(s-1) g q_{biVol}}{F_i (u^{*'})^3}, \quad (11)$$

where s is the relative sediment density ($s = \rho_s/\rho$), ρ_s is the sediment density (2650 kg m^{-3}), ρ is the water density, q_{biVol} is the volumetric fractional bedload transport rate per unit width (m^3 s^{-1} m^{-1}), F_i is the

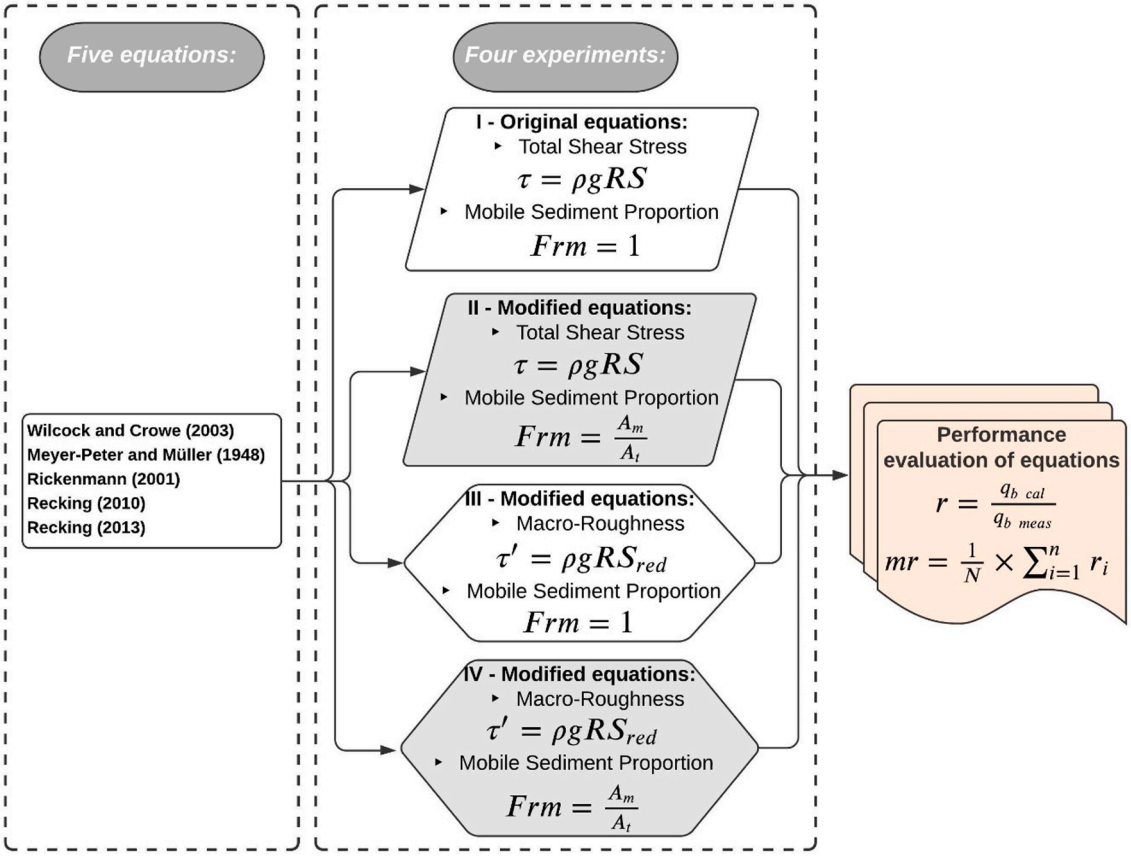

Fig. 6. Schematic overview of five bedload transport equations employed in four experiments. In the experiments, the same shape characterized total (τ) or reduced shear stress ($\tau^{'}$), and the same hatch color described whether the mobile sediment proportion (*Frm*) was used.

proportion grain size class i obtained from the GSD of the bed surface, and $u^{*\prime}$ is the shear velocity with the reduced shear stress $\left(u^{*'} = [\tau^{'}/\rho]^{0.5}\right)$.

$$W_i^{*'} = \begin{cases} 0.002(\tau^{'}/\tau_{ri})^{7.5} & (\tau^{'}/\tau_{ri}) < 1.35 \\ 14\left(1 - \dfrac{0.894}{(\tau^{'}/\tau_{ri})^{0.5}}\right)^{4.5} & (\tau^{'}/\tau_{ri}) \geq 1.35 \end{cases} \tag{12}$$

The reference shear stress (τ_{ri}) of each grain-size fraction (D_i) was determined as a function of the median grain size (D_{50}) and the reference shear stress of the mean grain size(τ_{rDm}), as shown in Eq. (13) and by the exponent b in Eq. (14).

$$\tau_{ri} = \tau_{rDm}\left(\frac{D_i}{D_{50}}\right)^{b} \tag{13}$$

$$b = \frac{0.67}{1 + exp\left(1.5 - \frac{D_i}{D_{50}}\right)} \tag{14}$$

We used the τ_{rDm} value calculated from the dimensionless reference shear stress ($\tau^{*}_{rDm} = 0.03$). This value has already been adopted in other studies, and additional resistance was considered due to macro-roughness (Schneider et al., 2016, 2015a). The total unit bedload transport rate is the sum of the fractions of each of the classes i (Eq. (15)):

$$q_b = \sum\left(\frac{W_i^{*'} F_i (u^{*'})^3}{(s-1)g}\right)\rho_s\left(\frac{A_m}{A_{tot}}\right), \tag{15}$$

where q_b is the total unit bedload transport rate (kg s^{-1} m^{-1}).

The equation of Meyer-Peter and Müller (1948) (MPM-1948) has a constant dimensionless critical shear stress ($\tau^{*}_{c} = 0.047$) in its original formulation. To consider the effects of macro-roughness ($\tau^{*'}_{c}$), we used the same method as Heimann et al. (2015) and Rickenmann (2018), combining the empirical equation of Lamb et al. (2008) with the reduction factor $\left(\tau^{*'}_{c} = [0.15S^{0.25}]S_{red}/S\right)$. The MPM-1948 equation was as follows:

$$q_b = 8\rho_s\sqrt{g(s-1)D_{50}^{3}}\left[\left(\frac{n^{'}}{n}\right)^{3/2}\tau^{*'} - \tau^{*'}_{c}\right]^{3/2}\left(\frac{A_m}{A_{tot}}\right), \tag{16}$$

where

n is the reduced roughness coefficient (Manning coefficient considering S_{red}), n was estimated by the equation $\left(n = S_{red}^{1/2}R^{2/3}/v\right)$;

n' represents the grain roughness, n' was calculated using the equation from Strickler (1923) $\left(n^{'} = D_{90}^{1/6}/26\right)$, and; v is the mean flow velocity (m s^{-1}).

The equation of Rickenmann (2001) (Rn-2001) was developed using data from 252 laboratory experiments and had bed slopes from 0.0004 to 0.2 m m^{-1}.

$$\Phi_b = 3.1\left(\frac{D_{90}}{D_{30}}\right)^{0.2}\sqrt{\tau^{*'}}(\tau^{*'} - \tau^{*'}_{c})Fr\frac{1}{\sqrt{s-1}} \tag{17}$$

$$\Phi_b = \frac{q_{bVol}}{\sqrt{(s-1)gD_{50}^{3}}} \tag{18}$$

$$q_b = q_{bVol}\rho_s\sqrt{(s-1)gD_{50}{}^3}\left(\frac{A_m}{A_{tot}}\right) \quad (19)$$

In Eqs. (17)–(19):

Φ_b is the dimensionless bedload transport rate;
D_{90} and D_{30} are the diameters with 90% and 30% of the granulometry of the finer bed surface, respectively;
q_{bVol} is the volumetric bedload transport rate per unit width ($m^3\ s^{-1}\ m^{-1}$), and;
Fr is the Froude number $\left(Fr = v/\sqrt{gR}\right)$.

The equation of Recking (2010) (Rg-2010) was developed to estimate the total bedload transport rate using data from 84 river reaches obtained from laboratory and field experiments. The equation Rg-2010 uses D_{84} to calculate the dimensionless reduced shear stress $(\tau^{*'}{}_{84})$and the dimensionless reduced critical shear stress $(\tau^{*'}{}_{c84})$.

$$\tau^{*'}{}_{c84} = (1.32S_{red} + 0.037)\left(\frac{D_{84}}{D_{50}}\right)^{-0.93} \quad (20)$$

$$\tau^{*'}{}_{m} = 12.53\left(\frac{D_{84}}{D_{50}}\right)^{-4.445\sqrt{S_{red}}}(\tau^{*'}{}_{c84})^{1.605} \quad (21)$$

$$\tau^{*'}{}_{84} = \frac{\tau'}{(\rho_s - \rho)gD_{84}} \quad (22)$$

$$\Phi_b = \begin{cases} 0.0005\left(\frac{D_{84}}{D_{50}}\right)^{-18\sqrt{S_{red}}}\left(\frac{\tau^{*'}{}_{84}}{\tau^{*'}{}_{c84}}\right)^{6.5} & (\tau^{*'}{}_{84}) < (\tau^{*'}{}_{m}) \quad (1) \\ 14(\tau^{*'}{}_{84})^{2.45} & (\tau^{*'}{}_{84}) \geq (\tau^{*'}{}_{m}) \quad (2) \end{cases} \quad (23)$$

$$q_b = q_{bVol}\rho_s\sqrt{(s-1)gD_{84}{}^3}\left(\frac{A_m}{A_{tot}}\right) \quad (24)$$

where $(\tau^{*'}{}_{m})$ corresponds to the intersection between Eqs. (23.1) and (23.2), providing a transition between partial transport and full mobility (Recking, 2013).

The model developed by Recking (2013) (Rg-2013) differs from Recking (2010) as the former combines Eqs. (23.1) and (23.2) into a single continuous function (Eq. (25)).

$$\Phi_b = \frac{14(\tau^{*'}{}_{84})^{2.5}}{\left(1 + \left(\frac{\tau^{*'}{}_{m}}{\tau^{*'}{}_{84}}\right)^4\right)} \quad (25)$$

$$\tau^{*'}{}_{m} = \begin{cases} (5S_{red} + 0.06)\left(\frac{D_{84}}{D_{50}}\right)^{4.5\sqrt{S_{red}}-1.5} & For\ gravel \\ 0.045 & For\ sand \end{cases} \quad (26)$$

$$q_b = q_{bVol}\rho_s\sqrt{(s-1)gD_{84}{}^3}\left(\frac{A_m}{A_{tot}}\right) \quad (27)$$

2.9. Evaluation of bedload transport equation performances

We compared the measured ($q_{b\ meas}$) and computed ($q_{b\ cal}$) unit bed load transport rate. A graphical method and index based on the discrepancy ratio were used to evaluate the performances of the equations ($r = q_{b\ cal}/q_{b\ meas}$). The index r was then grouped into two intervals in which the $q_{b\ cal}$ values fell within one order of magnitude ($0.1 < r < 10$) and within two orders of magnitude ($0.01 < r\ (100)$ about $q_{b\ meas}$ values. This methodology is widely used to evaluate the performance of bedload transport equations (Habersack and Laronne, 2002; López et al., 2014; Recking, 2010; Recking et al., 2012; Schneider et al., 2016, 2015a; Vázquez-Tarrío and Menéndez-Duarte, 2015). Additionally, the arithmetic mean of r (mr) was calculated according to Eq. (28):

$$mr = \frac{1}{N} \times \sum_{i=1}^{N} r_i, \quad (28)$$

where N is the number of data points and r_i is the ith value of r. This interval varies from 0 to $+\infty$, with values close to 1 indicating less discrepancy.

Finally, in graphical form, the relationship between $q_{b\ cal}$ and $q_{b\ meas}$ was evaluated, and the index discrepancy (r) was used to analyze the distribution for each equation using a boxplot.

3. Results and discussion

3.1. Flow resistance analysis

The flow resistance laws described in the Section 2.5 (and many others not mentioned here) were developed for flow conditions in alluvial channels. For better analysis, we compared the measured data from the reach of Arroio do Ouro (mixed bedrock–alluvial channel) to an extensive compilation of alluvial channel data obtained by Rickenmann and Recking (2011) and to the data measured by David et al. (2010b) in steep mountain streams (Fig. 7). The prediction equations developed by Rickenmann and Recking (2011) (Eq. (5) and Eq. (21b) in Rickenmann and Recking, 2011) and the original VPE (Eq. (3)) are also shown in Fig. 7.

The Arroio do Ouro data plots below the limit of the observed range of alluvial flow resistance was overlaid with the data presented by David et al. (2010b) in the mountain stream reaches (Fig. 7a). The high proportion of boulder patches in this reach (14%; see Table 1) added to the bedrock protrusion (see Fig. 2) is important because flow resistance mainly results from macro-roughness, including the drag that occurs around large boulders (Nitsche et al., 2012). This was indicated by Ferguson et al. (2017a), who verified that a reach of bedrock with 70% alluvial cover and 11% of boulder density was also below the limit of $(8/f_{tot})^{0.5}$ that is observed for alluvial channels. It is evident that the equations developed for coarse-bed alluvial channels underestimate the measured flow resistance in the reach of Arroio do Ouro (Fig. 7a).

Similarly, as observed by the Darcy–Weisbach relationships (Fig. 7a), the Arroio do Ouro data plot is below the limit of the data compiled by Rickenmann and Recking (2011) when expressing the relationship using flow velocity (v^{**}), which is dimensionless, and unit discharge (q^{**}) (Fig. 7b). The small prefactor k (Eq. (4)) value implies a higher flow resistance (additional roughness sources) that was not considered when Rickenmann and Recking (2011) developed Eq. (5). Even data collected by David et al. (2010b) in alluvial channels had the sources of additional roughness, resulting in behavior similar to our data. As woody debris is present in many reaches, as measured by David et al. (2010b), it can be assumed that the high flow resistance could be influenced by the increasing wood load. In the studied reach, we observed that large borders and bedrock protrusion were important for flow resistance; in contrast, woody debris was unimportant as a source of roughness (see Fig. 2).

As expected from the analysis of Fig. 7, the Rickenmann and Recking (2011) equations and the original VPE equation (Ferguson, 2007) strongly overestimated the flow velocity (Fig. 8). Despite this, the dimensionless hydraulic geometry approach provides better flow velocity predictions than the Darcy–Weisbach relationships. This was also observed when the power-law equations were fitted to data (Fig. 8).

3.2. Bedload transport rating curves

The measured bedload transport rate in the Arroio do Ouro stream ranged between 0.05 and 3.63 kg s^{-1} for the observed discharge range of 1.6–14.8 $m^3\ s^{-1}$ (Table S1, supplementary material). The shear stress (τ) presented range values of 91.6–219.7 Pa, while the reduced shear stress

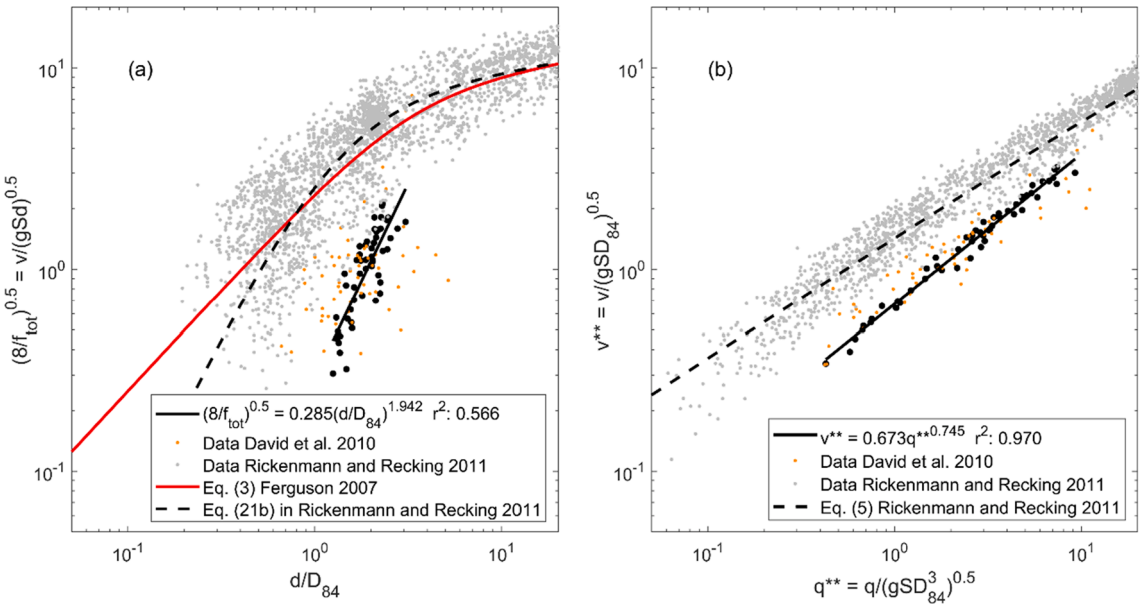

Fig. 7. (a) Relationship between flow resistance and relative flow depth; (b) dimensionless velocity related to dimensionless discharge. Grey dots represent Rickenmann and Recking (2011) data. Orange dots represent David et al. (2010b) data. Rickenmann and Recking (2011) equations are shown by black dashed lines. The thick red line shows the variable power equation (VPE) given by Ferguson (2007). Black lines show power-law equations as fitted to the data (black dots). (For interpretation of the references to color in this figure legend, the reader is referred to the web version of this article.)

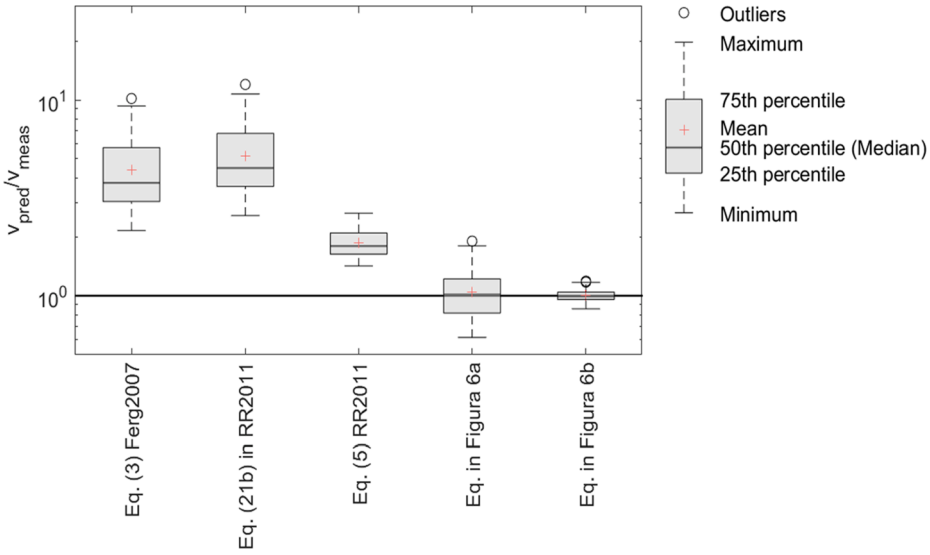

Fig. 8. Measured flow velocity (v_{meas}) compared to velocity predictions (v_{pred}) based on relative flow depth and dimensionless discharge. Black line indicates a perfect fit. Eq. (3) is a variable power equation VPE from Ferguson (2007) (Ferg2007) and Eq. (21b) and (5) were developed by Rickenmann and Recking (2011) (RR2011). Power-law equations, fitted for the Arroio do Ouro data and given in Fig. 7, are included.

($\tau^{'}$)values represent a mean reduction of approximately three times (11.3–95.3 Pa) compared to τ. The difference between τ and $\tau^{'}$ increases as the mean flow depth decreases because the resistance caused by the macro-roughness is represented by a function of the relative flow depth (d/D_{84}) (Rickenmann and Recking, 2011). During the measurements, the relative flow depth presented reduced values ($1.25 < d/D_{84} < 3.1$) (Fig. 7a), highlighting the importance of considering large elements (such as boulders and bedrock protrusion) in determining the GSD of bed material.

The adjustment curve between the bedload transport rate (Q_b) and discharge (Q) was described by a power function ($Q_b = aQ^b$) with an exponent b ($b = 2.149$) (Fig. 9; Eq. (29)). In this power function, the exponent indicates the steepness of the curve. Steeper curves have a higher rate of increase in the transport rate with increasing flow (Bunte et al., 2006).

$$Q_b = 0.017Q^{2.149}r^2 = 0.73 \quad (29)$$

where Q_b (kg s^{-1}) is the measured bedload transport rate, Q (m^3 s^{-1}) is the discharge rate, and r^2 is the coefficient of determination.

An exponent of approximately 2.15 represents less steep rating curves and is often related to the particle sizes and the type of sampler used. High rating curve exponent values were observed in rivers which transport coarser grains such as gravel and small cobbles. Schneider et al. (2016) also found a high exponent value (6.3) in a mountain stream in Switzerland, considering only bedload transport with D > 4 mm. As noticed by Bunte et al. (2008), when the Helley–Smith sampler

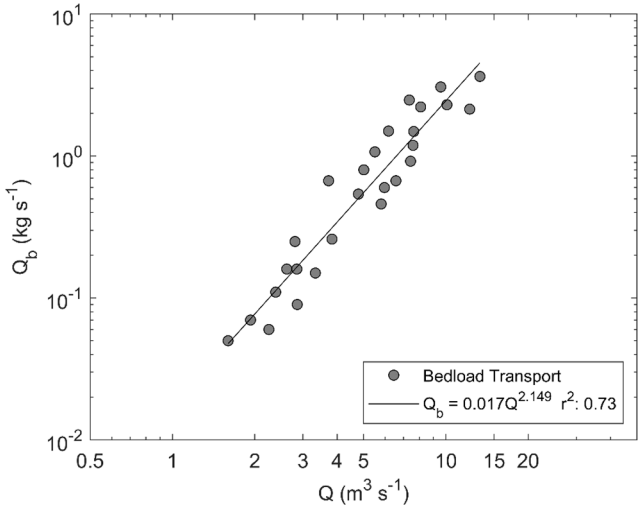

Fig. 9. Power function rating curve between the measured bedload transport rate (Q_b) and discharge (Q).

was used to estimate the transport in rivers with gravel bed material, it reproduced much higher transport rates during low flows, and the increased discharge generated less steep curves with exponents of 2–4 (Bunte et al., 2008).

3.3. Performance of equations using the four tested approaches

When we considered the macro-roughness effects (calculated from the reduced energy slope [S_{red}] and the limited availability of bed sediment [A_m/A_{tot}]), all five equations showed improved performance in predicting the bedload transport rates (Table 2; Fig. 10). The performances of the five tested equations for each of the 27 measurements of bedload transport are provided in the supplementary material (Table S2).

Table 2
Statistical index values used to assess bedload transport equations.

Equation	r (0.1–10)[a] (%)	r (0.01–100)[b] (%)	mr (-)[c]
I – Original equations			
MPM-1948 (Eq. S7)	0.0	100.0	30.2
Rg-2013 (Eq. S13–S15)	0.0	55.6	146.9
Rg-2010 (Eq. S8–S12)	0.0	44.4	188.3
Rn-2001 (Eq. S16–S18)	0.0	0.0	450.9
WC-2003 (Eq. S1–S6)	0.0	0.0	6989.6
II – Modified equations (τ and *Frm*)			
MPM-1948 (Eq. S20)	11.1	100.0	22.3
Rg-2013 (Eq. S22)	0.0	66.7	108.7
Rg-2010 (Eq. S21)	0.0	59.3	139.3
Rn-2001 (Eq. S23)	0.0	11.1	333.6
WC-2003 (Eq. S19)	0.0	0.0	5172.1
III – Modified equations (τ')			
Rg-2013 (Eq. S32–S33)	77.8	100	7.5
Rg-2010 (Eq. S28–S31)	63.0	100	9.7
MPM-1948 (Eq. S27)	18.5	100	18.9
WC-2003 (Eq. S24–S26)	0.0	77.8	73.4
Rn-2001 (Eq. S34)	0.0	70.4	75.4
IV – Modified equations (τ' and *Frm*)			
Rg-2013 (Eqs. (25)–(27))	85.2	100.0	5.6
Rg-2010 (Eqs. (20)–(24))	77.8	100.0	7.2
MPM-1948 (Eq. (16))	37.0	100.0	14.0
Rn-2001 (Eqs. (17)–(19))	0.0	92.6	55.8
WC-2003 (Eqs. (11)–(15))	0.0	88.9	54.3

[a] $0.1 < r < 10$, the percentage of the estimated transport rate that does not exceed 10 times (one order of magnitude) higher than the observations.
[b] $0.01 < r < 100$, the percentage of estimated transport rate that does not exceed 100 times (two orders of magnitude) higher than the observations.
[c] Mean of r; the closer to 1, the smaller the discrepancy.

Table 2 describes the statistical indices, considering the original equations and the three analyzed modifications. We classified the values in an ascending order of increasing discrepancy between the total bedload transport rate estimated by the equations and those measured in the field. As we used a constant reduction factor of the available bed material (*Frm* = 0.74), this represents a 26% reduction in the bedload transport rate calculated from the original equations. We also observed that using reduced shear stress (τ') was much more significant for improving the equations (i.e., resulting in an average reduction in the bedload transport rate by 80%).

Thus, for the Arroio do Ouro reach, the implementation of τ' proved to be more critical for improving the performance of the equations than the use of only *Frm*. It should be noticed that in mixed bedrock–alluvial channels, the proportion of alluvial cover in the bed varies in different reaches (Ferguson et al., 2017a; Hodge et al., 2011). In addition, to consider the use of *Frm* in bedload transport equations, temporal dynamics may be important. Extreme flood events cause the changes in both the GSD and the availability of bed material that can be transported (Turowski et al., 2013).

We obtained optimal results for estimating the bedload transport rate when we used τ' and *Frm* together in the equations (see IV- modified equations; Table 2). Even though we presented the two approaches separately, we were unable to dissociate their analysis in the scenarios of mixed bedrock–alluvial channels. Recent studies based on experimental measures have shown that hydraulic resistance changes with the degree of alluviation (Fernández et al., 2020) and that bed roughness is an essential factor in controlling alluvial cover (Mishra and Inoue, 2020).

In general, the accuracy of bedload transport equations depends to a great extent on whether the energy losses due to macro-roughness are considered (Figs. 10 and 11). However, all our results indicate that this energy loss (considered by flow resistance equations) was underestimated for the flow characteristics of mixed bedrock–alluvial channels (Figs. 6 and 7). This was also observed by Ferguson et al. (2017a) in a reach that has some exposed bedrock and many boulders.

Alternative methods may be applied to investigate other approaches to estimate the bed roughness height. By analyzing an extensive dataset compiled from flume experiments and field measurements, better results were obtained in predicting the flow velocity using the standard deviation of bed elevation (σ_z) as a roughness descriptor in gravel bed streams (Chen et al., 2020). Ferguson et al. (2019) also presented promising results using σz as the roughness height in a small bedrock reach with negligible sediment cover. However, was analyzed the use of σ_z for a relatively smooth rock bed, there is a gap in the research conducted in instances wherein the bed conditions are irregular (Ferguson et al., 2019), as observed in the Arroio do Ouro reach. In addition to σ_z, other parameters related to surface roughness can be considered more appropriate for evaluating flow resistance than the grain size of bed material. Similarly, grain protrusion proved to be adequate for assessing the stability of a gravel bed (Hodge et al., 2020).

3.4. Analyses of bedload transport equations

Optimal performances (considering the effects of macro-roughness and the limited availability of mobile sediment) were obtained using the equations of Recking (2013, 2010), followed by the equation of Meyer-Peter and Müller (1948) (Table 2). In these equations, the predicted bedload transport rate did not exceed two orders of magnitude and overestimated the bedload transport rate by up to 14 times (Table 2; Fig. 10). The other two equations (Rickenmann, 2001; Wilcock and Crowe, 2003) presented lower performances with arithmetic mean of r (mr) values > 50 indicating over-predictions of the bedload transport rate.

When we analyzed the original equations or considered only the *Frm*, the Meyer-Peter and Müller (1948) equation best estimated the bedload transport, with 100% of the values in the range of $0.01 < r < 100$. The

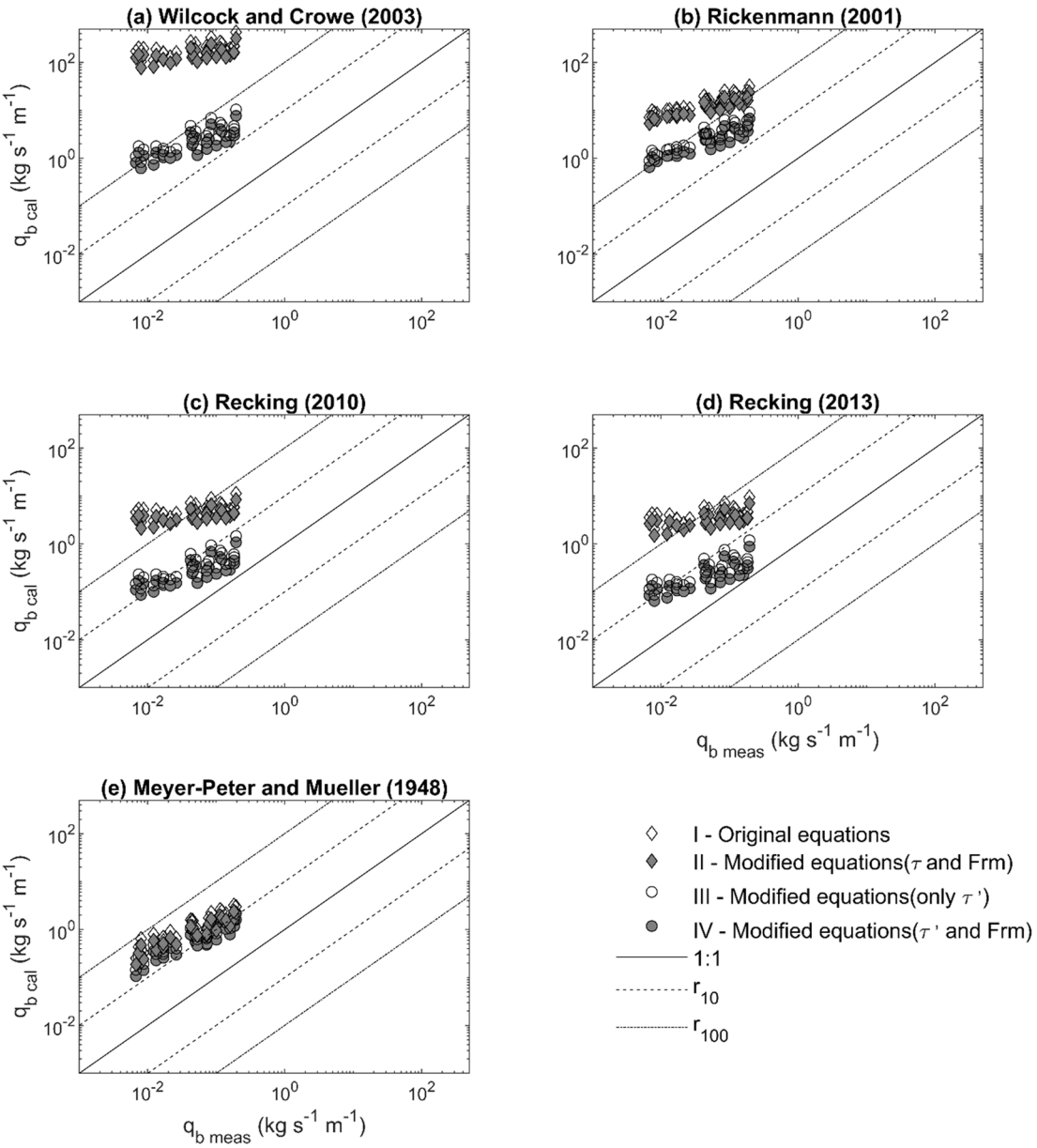

Fig. 10. Comparison between unit bedload transport rates (i.e., measured [$q_{b\ meas}$] and estimated [$q_{b\ cal}$]), calculated using five different equations tested in four experiments. The parallel solid line represents a perfect fit ($r = 1$), dashed lines correspond to the interval $0.1 < r < 10$, and dash-dotted lines represent the interval $0.01 < r < 100$.

other equations overestimated the bedload transport rates by mean of two (Rg-2013, Rg-2010, and Rn-2001; Table 2) to three orders of magnitude (WC-2003; Table 2) in both situations. The good performance of the original MPM-1948 equation may be associated with a method that partitions the shear stress (n'/n; ratio of particle roughness n' to total roughness n), which corrects the total boundary shear stress to the skin friction stress (Barry et al., 2004; Recking, 2010; Recking et al., 2012). Testing 10 bedload transport equations in the Ebro River, López et al. (2014) verified that the MPM-1948 equation exhibited an unreliable performance because it overestimated the bedload transport rate. According to them, this may have occurred because of the use of the plane-bed hypothesis ($n'/n = 1$). However, we did not use this hypothesis and the n'/n values were < 1, with n calculated using Manning's equation and n' calculated using Strickler's equation (1923).

When energy losses were neglected (Figs. 10a and 11a and b), the Wilcock and Crowe (2003) equation exhibited the lowest performance among all the equations used in this study. A poor performance was also observed by Schneider et al. (2015a) when using the Wilcock and Crowe (2003) equation without considering macro-roughness in an extensive field dataset. In two reaches of a mountain stream in Switzerland, the WC-2003 equation overestimated the bedload transport rate by more than six orders of magnitude when the energy losses due to macro-roughness were neglected (Schneider et al., 2016). Similar to the present study, Schneider et al. (2015a, 2016) found significant improvements in the bedload transport rate estimates when WC-2003 was used with reduced shear stress (τ').

The predicted bedload transport rates calculated using the equation of Rickenmann (2001) (Rn-2001) exceeded one order of magnitude when considering the macro-roughness effects and the limited mobility of the sediments, and, on average, exceeded the original equations by two orders of magnitude (Figs. 10b and 11a). By analyzing bedload transport in two streams in southern Columbia Mountains in Canada, Green et al. (2015) observed that the Rickenmann (2001) equation also had a poor performance, overpredicting transport rates by up to two

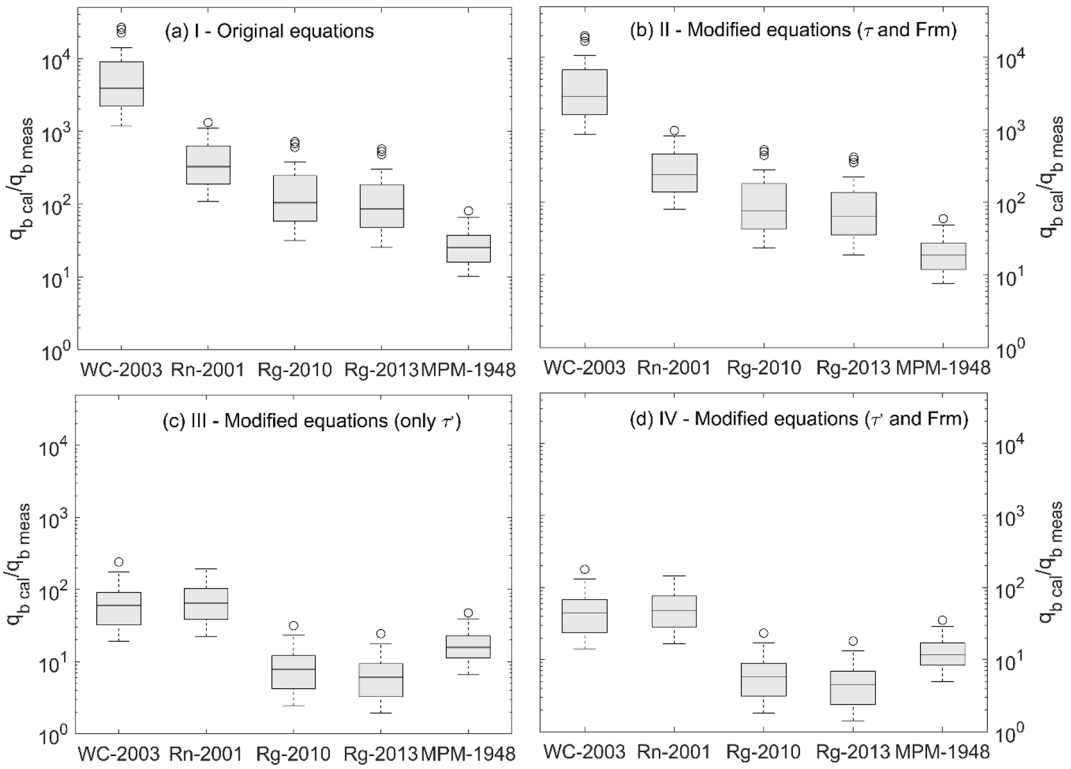

Fig. 11. Discrepancy ratios ($r = q_{b\ cal}/q_{b\ meas}$) between estimated ($q_{b\ cal}$) and measured ($q_{b\ meas}$) unit bedload transport rates for five different equations tested in four experiments: (a) I – Original equations, (b) II – Modified equations (τ and *Frm*), (c) III- Modified equations (only $\tau^{'}$), and (d) IV- Modified equations ($\tau^{'}$ and *Frm*).

orders of magnitude. Even though the Rn-2001 equation has lower applicability than the other equations tested in this study, the overestimation in the Rn-2001 equation is reduced by approximately eight times when macro-roughness and reduced bed mobility are considered. The equation was developed from experimental laboratory data using uniform sediment cover, thereby overestimating the bedload transport rates in the mixed bedrock–alluvial channel.

The Recking (2013) and Recking (2010) equations obtained the most accurate estimates among all the equations used in this study. The authors elaborated on the equations using a large set of field and laboratory data for sand and gravel-bed rivers with slopes of 0.0002–0.08 m m^{-1} (Recking, 2010). Recking et al. (2012) obtained a good performance (i.e., 78% in the range of $0.1 < r < 10$) using the Rg-2010 equation. Both equations (Rg-2013 and Rg-2010) use D_{84}, because this diameter is used with bed roughness in flow resistance equations (Rickenmann and Recking, 2011) and because the mobility parameter ($\tau^{*'}{}_m$; Eqs. (21) and (26)) can be considered as the transition between full mobility and partial transport of the sediment mixture (Recking et al., 2012).

4. Conclusions

We analyzed the bedload transport rate and the performances of five bedload equations in a mixed bedrock–alluvial stream in Southern Brazil. To consider the energy loss effects caused by the macro-roughness of large elements (such as boulders), we combined the flow resistance equation with bedload transport equations that used a reduced energy slope. We also applied a reduction factor of the available bed material in the bedload transport equations because the reach investigated in the study was partially covered with large elements of roughness that were not available to be transported. The bedload transport was limited to particles with fine granulometry (from fine-grained sand to medium-sized gravel), as evidenced by the magnitude of the exponent "b" (2.15) that described the ratio of the discharge to the bedload transport rate.

All five equations showed improved performances in predicting bedload transport rates when the macro-roughness effects calculated from the reduced energy slope and the limited availability of bed sediments were considered. The best performance was obtained using the Recking (2013) equation, in which 85.2% of the bedload transport rate estimates did not exceed one order of magnitude ($r < 10$) relative to the observed data. By analyzing the equations separately, we conclude that the implementation of reduced shear stress proved to be more critical for improving the performance of the equations than the use of the proportion of mobile sediments.

It is important to highlight that even when combining flow resistance equations with the available bed material, the equations overestimated the bedload transport rate in the studied reach. This indicates that the energy loss considered in flow resistance equations is underestimated for the flow characteristics of mixed bedrock–alluvial channels. Therefore, our results provide evidence that energy loss caused by large boulders and bedrock protrusions should be reviewed in flow resistance equations in future studies. A valuable addition may be the investigation of different methods to estimate the bed roughness height.

Declaration of Competing Interest

The authors declare that they have no known competing financial interests or personal relationships that could have appeared to influence the work reported in this paper.

Acknowledgments

The authors wish to thank NEPE-HidroSedi at Federal University of Pelotas (UFPel) for offering us its facilities to perform lab analysis and field campaigns. We thank Dieter Rickenmann for providing flow resistance data compiled by Rickenmann and Recking (2011). We would also like to thank the associate editor and two anonymous reviewers

whose comments contributed to improving the manuscript. We thank the National Council for Scientific and Technological Development (CNPq) for financing a PhD fellowship (Grant number 141235/2017-9) for the first author and research productivity fellowship for the second and fourth authors (Grant number 305636/2019-7).

Appendix A. Supplementary material

Supplementary data to this article can be found online at https://doi.org/10.1016/j.catena.2020.105108.

References

Barry, J.J., Buffington, J.M., King, J.G., 2004. A general power equation for predicting bed load transport rates in gravel bed rivers. Water Resour. Res. 40, 1–22. https://doi.org/10.1029/2004WR003190.

Bartels, G.K., Terra, V.S.S., Cassalho, F., Lima, L.S., Reinert, D.J., Collares, G.L., 2016. Spatial variability of soil physical and hydraulic properties in the southern Brazil small watershed. African J. Agric. 11, 5036–5042. https://doi.org/10.5897/AJAR2016.11812.

Bathurst, J.C., Li, R.-M., Simons, D.B., 1981. Resistance equation for large-scale roughness. J. Hydraul. Div. 107, 1593–1613.

Buffington, J.M., Montgomery, D.R., 1999. A procedure for classifying textural facies in gravel-bed rivers. Water Resour. Res. 35, 1903–1914. https://doi.org/10.1029/1999WR900041.

Bunte, K., Abt, S.R., 2001. Sampling frame for improving pebble count accuracy in coarse gravel-bed streams. JAWRA J. Am. Water Resour. Assoc. 37, 1001–1014. https://doi.org/10.1111/j.1752-1688.2001.tb05528.x.

Bunte, K., Abt, S.R., Potyondy, J.P., Swingle, K.W., 2009. Comparison of three pebble count protocols (Emap, Pibo, and Sft). J. Am. Resour. Assoc. 45, 1209–1227.

Bunte, K., Abt, S.R., Potyondy, J.P., Swingle, K.W., 2008. A comparison of coarse bedload transport measured with bedload traps and Helley-Smith samplers. Geodin. Acta 21, 53–66. https://doi.org/10.3166/ga.21.53-66.

Bunte, K., Abt, S.R., Swingle, K.W., 2006. Predictability of bedload rating and flow competence curves from bed armoring, stream width and basin area. In: PROCEEDINGS of the Eight Federal Interagency Sedimentation Conference (8thFISC). FISC, Reno, NV, USA, pp. 98–106.

Chatanantavet, P., Parker, G., 2008. Experimental study of bedrock channel alluviation under varied sediment supply and hydraulic conditions. Water Resour. Res. 44, 1–19. https://doi.org/10.1029/2007WR006581.

Chen, X., Hassan, M.A., An, C., Fu, X., 2020. Rough correlations: meta-analysis of roughness measures in gravel bed rivers. Water Resour. Res. 56, 1–19. https://doi.org/10.1029/2020WR027079.

Comiti, F., Mao, L., 2012. Recent advances in the dynamics of steep channels. In: Church, M., Biron, P.M., Roy, A.G. (Eds.), Gravel-Bed Rivers. John Wiley & Sons, Ltd, Chichester, UK, pp. 351–377. https://doi.org/10.1002/9781119952497.ch26.

Comiti, F., Mao, L., Wilcox, A., Wohl, E.E., Lenzi, M.A., 2007. Field-derived relationships for flow velocity and resistance in high-gradient streams. J. Hydrol. 340, 48–62. https://doi.org/10.1016/j.jhydrol.2007.03.021.

David, G.C.L., Wohl, E., Yochum, S.E., Bledsoe, B.P., 2010a. Controls on at-a-station hydraulic geometry in steep headwater streams, Colorado, USA. Earth Surf. Process. Landforms 35, 1820–1837. https://doi.org/10.1002/esp.2023.

David, G.C.L., Wohl, E., Yochum, S.E., Bledsoe, B.P., 2010b. Controls on spatial variations in flow resistance along steep mountain streams. Water Resour. Res. 46, 1–21. https://doi.org/10.1029/2009WR008134.

Emmett, W.W., 1980. A Field Calibration of the Sediment-Trapping Characteristics of the Helley-Smith Bedload Sampler. US Government Printing Office, Washington, D.C.

Ferguson, R., 2007. Flow resistance equations for gravel- and boulder-bed streams. Water Resour. Res. 43, 1–12. https://doi.org/10.1029/2006WR005422.

Ferguson, R.I., Hardy, R.J., Hodge, R.A., 2019. Flow resistance and hydraulic geometry in bedrock rivers with multiple roughness length scales. Earth Surf. Process. Landforms 44, 2437–2449. https://doi.org/10.1002/esp.4673.

Ferguson, R.I., Sharma, B.P., Hardy, R.J., Hodge, R.A., Warburton, J., 2017a. Flow resistance and hydraulic geometry in contrasting reaches of a bedrock channel. Water Resour. Res. 53, 2278–2293. https://doi.org/10.1002/2016WR020233.

Ferguson, R.I., Sharma, B.P., Hodge, R.A., Hardy, R.J., Warburton, J., 2017b. Bed load tracer mobility in a mixed bedrock/alluvial channel. J. Geophys. Res. Earth Surf. 122, 807–822. https://doi.org/10.1002/2016JF003946.

Fernández, R., Vitale, A.J., Parker, G., García, M.H., 2020. Hydraulic resistance in mixed bedrock-alluvial meandering channels. J. Hydraul. Res. 1–16 https://doi.org/10.1080/00221686.2020.1780489.

Food and Agriculture Organization of the United Nations, 2014. World reference base for soil resources 2014: International soil classification system for naming soils and creating legends for soil maps. FAO, Rome.

Green, K., Alila, Y., Brardinoni, F., 2015. Patterns of bedload entrainment and transport in forested headwater streams of the Columbia Mountains Canada. Earth Surf. Process. Landforms 40, 427–446. https://doi.org/10.1002/esp.3642.

Habersack, H.M., Laronne, J.B., 2002. Evaluation and improvement of bed load discharge formulas based on Helley-Smith sampling in an alpine gravel bed river. J. Hydraul. Eng. 128, 484–499. https://doi.org/10.1061/(ASCE)0733-9429(2002)128:5(484).

Heimann, F.U.M., Rickenmann, D., Turowski, J.M., Kirchner, J.W., 2015. sedFlow – a tool for simulating fractional bedload transport and longitudinal profile evolution in mountain streams. Earth Surf. Dyn. 3, 15–34. https://doi.org/10.5194/esurf-3-15-2015.

Helley, E.J., Smith, W., 1971. Development and calibration of a pressure difference bedload sampler. USGS Water Resources Division Open-file report.

Hodge, R.A., Hoey, T.B., 2012. Upscaling from grain-scale processes to alluviation in bedrock channels using a cellular automaton model. J. Geophys. Res. Earth Surf. 117 https://doi.org/10.1029/2011JF002145.

Hodge, R.A., Hoey, T.B., Sklar, L.S., 2011. Bed load transport in bedrock rivers: the role of sediment cover in grain entrainment, translation, and deposition. J. Geophys. Res. 116, F04028. https://doi.org/10.1029/2011JF002032.

Hodge, R.A., Voepel, H., Leyland, J., Sear, D.A., Ahmed, S., 2020. X-ray computed tomography reveals that grain protrusion controls critical shear stress for entrainment of fluvial gravels. Geology 48, 149–153. https://doi.org/10.1130/G46883.1.

Inoue, T., Izumi, N., Shimizu, Y., Parker, G., 2014. Interaction among alluvial cover, bed roughness, and incision rate in purely bedrock and alluvial-bedrock channel. J. Geophys. Res. Earth Surf. 119, 2123–2146. https://doi.org/10.1002/2014JF003133.

Johnson, J.P.L., 2014. A surface roughness model for predicting alluvial cover and bed load transport rate in bedrock channels. J. Geophys. Res. Earth Surf. 119, 2147–2173. https://doi.org/10.1002/2013JF003000.

Lamb, M.P., Dietrich, W.E., Venditti, J.G., 2008. Is the critical shields stress for incipient sediment motion dependent on channel-bed slope? J. Geophys. Res. Earth Surf. 113, 1–20. https://doi.org/10.1029/2007JF000831.

López, R., Vericat, D., Batalla, R.J., 2014. Evaluation of bed load transport formulae in a large regulated gravel bed river: the lower Ebro (NE Iberian Peninsula). J. Hydrol. 510, 164–181. https://doi.org/10.1016/j.jhydrol.2013.12.014.

Meyer-Peter, E., Müller, R., 1948. Formulas for bed-load transport. In: Proceedings of the 2nd Meeting of the International Association of Hydraulic Research. Stockholm, pp. 39–64. https://doi.org/1948-06-07.

Millar, R.G., 1999. Grain and form resistance in gravel-bed rivers Résistances de grain et de forme dans les rivières à graviers. J. Hydraul. Res. 37, 303–312. https://doi.org/10.1080/00221686.1999.9628249.

Mishra, J., Inoue, T., 2020. Alluvial cover on bedrock channels: applicability of existing models. Earth Surf. Dyn. 8, 695–716. https://doi.org/10.5194/esurf-8-695-2020.

Monsalve, A., Yager, E.M., Turowski, J.M., Rickenmann, D., 2016. A probabilistic formulation of bed load transport to include spatial variability of flow and surface grain size distributions. Water Resour. Res. 52, 3579–3598. https://doi.org/10.1002/2015WR017694.

Nitsche, M., Rickenmann, D., Kirchner, J.W., Turowski, J.M., Badoux, A., 2012. Macroroughness and variations in reach-averaged flow resistance in steep mountain streams. Water Resour. Res. 48, 1–16. https://doi.org/10.1029/2012WR012091.

Nitsche, M., Rickenmann, D., Turowski, J.M., Badoux, A., Kirchner, J.W., 2011. Evaluation of bedload transport predictions using flow resistance equations to account for macro-roughness in steep mountain streams. Water Resour. Res. 47 https://doi.org/10.1029/2011WR010645.

Peel, M.C., Finlayson, B.L., McMahon, T.A., 2007. Updated world map of the Köppen-Geiger climate classificatio. Hydrol. Earth Syst. Sci. 1, 1633–1644. https://doi.org/10.1127/0941-2948/2006/0130.

Philipp, R.P., Bom, F.M., Pimentel, M.M., Junges, S.L., Zvirtes, G., 2016a. SHRIMP U-Pb age and high temperature conditions of the collisional metamorphism in the V??rzea do Capivarita Complex: implications for the origin of Pelotas Batholith, Dom Feliciano Belt, southern Brazil. J. South Am. Earth Sci. 66, 196–207. https://doi.org/10.1016/j.jsames.2015.11.008.

Philipp, R.P., Pimentel, M.M., Chemale Jr, F., 2016b. Tectonic evolution of the Dom Feliciano Belt in Southern Brazil: geological relationships and U-Pb geochronology. Brazilian J. Geol. 46, 83–104. https://doi.org/10.1590/2317-4889201620150016.

Recking, A., 2013. Simple method for calculating reach-averaged bed-load transport. J. Hydraul. Eng. 139, 70–75. https://doi.org/10.1061/(ASCE)HY.1943-7900.0000653.

Recking, A., 2010. A comparison between flume and field bed load transport data and consequences for surface-based bed load transport prediction. Water Resour. Res. 46, 1–16. https://doi.org/10.1029/2009WR008007.

Recking, A., Liébault, F., Peteuil, C., Jolimet, T., 2012. Testing bedload transport equations with consideration of time scales. Earth Surf. Process. Landforms 37, 774–789. https://doi.org/10.1002/esp.3213.

Recking, A., Piton, G., Vazquez-Tarrio, D., Parker, G., 2016. Quantifying the morphological print of bedload transport. Earth Surf. Process. Landforms 41, 809–822. https://doi.org/10.1002/esp.3869.

Rickenmann, D., 2018. Variability of Bed load transport during six summers of continuous measurements in two Austrian Mountain Streams (Fischbach and Ruetz). Water Resour. Res. 54, 107–131. https://doi.org/10.1002/2017WR021376.

Rickenmann, D., 2012. Alluvial steep channels: flow resistance, bedload transport prediction, and transition to debris flows. In: Gravel-Bed Rivers. John Wiley & Sons, Ltd, Chichester, UK, pp. 386–397. https://doi.org/10.1002/9781119952497.ch28.

Rickenmann, D., 2001. Comparison of bed load transport in torrents and gravel bed streams. Water Resour. Res. 37, 3295–3305. https://doi.org/10.1029/2001WR000319.

Rickenmann, D., Recking, A., 2011. Evaluation of flow resistance in gravel-bed rivers through a large field data set. Water Resour. Res. 47 https://doi.org/10.1029/2010WR009793.

Schneider, J.M., Rickenmann, D., Turowski, J.M., Bunte, K., Kirchner, J.W., 2015a. Applicability of bed load transport models for mixed-size sediments in steep streams

considering macro-roughness. Water Resour. Res. 51, 5260–5283. https://doi.org/10.1002/2014WR016417.
Schneider, J.M., Rickenmann, D., Turowski, J.M., Kirchner, J.W., 2015b. Self-adjustment of stream bed roughness and flow velocity in a steep mountain channel. Water Resour. Res. 51, 7838–7859. https://doi.org/10.1002/2015WR016934.
Schneider, J.M., Rickenmann, D., Turowski, J.M., Schmid, B., Kirchner, J.W., 2016. Bed load transport in a very steep mountain stream (Riedbach, Switzerland): Measurement and prediction. Water Resour. Res. 52, 9522–9541. https://doi.org/10.1002/2016WR019308.
Sklar, L.S., Dietrich, W.E., 2004. A mechanistic model for river incision into bedrock by saltating bed load. Water Resour. Res. 40, 1–22. https://doi.org/10.1029/2003WR002496.
Strickler, K., 1923. Beiträge zur frage der geschwindigheits-formel und der rauhigkeitszahlen für strome, kanale und geschlossene leitungen, in: Eidgenössisches Amt Für Wasserwirtschaft. Eidgenössisches Amt für Wasserwirtschaft, Bern.
Turnipseed, D.P., Sauer, V.B., 2010. Discharge measurements at gaging stations, Techniques of Water-Resources Investigations of the United States Geological Survey. U.S. Geological Survey Techniques.
Turowski, J.M., Badoux, A., Leuzinger, J., Hegglin, R., 2013. Large floods, alluvial overprint, and bedrock erosion. Earth Surf. Process. Landforms 38, 947–958. https://doi.org/10.1002/esp.3341.
Turowski, J.M., Hovius, N., Wilson, A., Horng, M.-J., 2008. Hydraulic geometry, river sediment and the definition of bedrock channels. Geomorphology 99, 26–38. https://doi.org/10.1016/j.geomorph.2007.10.001.
Turowski, J.M., Lague, D., Hovius, N., 2007. Cover effect in bedrock abrasion: A new derivation and its implications for the modeling of bedrock channel morphology. J. Geophys. Res. 112, F04006. https://doi.org/10.1029/2006JF000697.
Vázquez-Tarrío, D., Menéndez-Duarte, R., 2015. Assessment of bedload equations using data obtained with tracers in two coarse-bed mountain streams (narcea river basin, NW spain). Geomorphology 238, 78–93. https://doi.org/10.1016/j.geomorph.2015.02.032.
Vericat, D., Church, M., Batalla, R.J., 2006. Bed load bias: Comparison of measurements obtained using two (76 and 152 mm) Helley-Smith samplers in a gravel bed river. Water Resour. Res. 42, 1–13. https://doi.org/10.1029/2005WR004025.
Whipple, K.X., DiBiase, R.A., Crosby, B.T., 2013. 9.28 Bedrock Rivers. In: Treatise on Geomorphology. Elsevier, pp. 550–573. https://doi.org/10.1016/B978-0-12-374739-6.00254-2.
Wilcock, P., Pitlick, J., Cui, Y., 2009. Sediment transport primer: estimating: estimating bed-material transport in gravel-bed rivers. U.S. Department of Agriculture, Forest Service, Rocky Mountain Research Station, Fort Collins, CO.
Wilcock, P.R., Crowe, J.C., 2003. Surface-based transport model for mixed-size sediment. J. Hydraul. Eng. 129, 120–128. https://doi.org/10.1061/(ASCE)0733-9429(2003)129:2(120).
Wohl, E., 2010. Mountain Rivers Revisited, Water Resources Monograph. American Geophysical Union, Washington, D.C. https://doi.org/10.1029/WM019.
Wolman, M.G., 1954. A method of sampling coarse river-bed material. Eos Trans. Am. Geophys. Union 35, 951–956. https://doi.org/10.1029/TR035i006p00951.
Yager, E.M., Dietrich, W.E., Kirchner, J.W., McArdell, B.W., 2012a. Patch dynamics and stability in steep, rough streams. J. Geophys. Res. Earth Surf. 117 https://doi.org/10.1029/2011JF002253.
Yager, E.M., Dietrich, W.E., Kirchner, J.W., McArdell, B.W., 2012b. Prediction of sediment transport in step-pool channels. Water Resour. Res. 48, 1–20. https://doi.org/10.1029/2011WR010829.
Yager, E.M., Kirchner, J.W., Dietrich, W.E., 2007. Calculating bed load transport in steep boulder bed channels. Water Resour. Res. 43, 1–24. https://doi.org/10.1029/2006WR005432.
Yuill, B., Nichols, M., Yager, E., 2010. Coarse bed material patch evolution in low-order, ephemeral channels. CATENA 81, 126–136. https://doi.org/10.1016/j.catena.2010.02.002.
Zhang, L., Parker, G., Stark, C.P., Inoue, T., Viparelli, E., Fu, X., Izumi, N., 2015. Macro-roughness model of bedrock–alluvial river morphodynamics. Earth Surf. Dyn. 3, 113–138. https://doi.org/10.5194/esurf-3-113-2015.
Zimmermann, A., 2010. Flow resistance in steep streams: an experimental study. Water Resour. Res. 46, 1–18. https://doi.org/10.1029/2009WR007913.